Journal of Alloys and Compounds 509 (2011) 2870–2873

Contents lists available at ScienceDirect

Journal of Alloys and Compounds

journal homepage: www.elsevier.com/locate/jallcom

Direct synthesis of Fe_3O_4 nanopowder by thermal decomposition of Fe–urea complex and its properties

S. Asuha*, B. Suyala, X. Siqintana, S. Zhao

Chemistry & Environment Science College, Inner Mongolia Normal University, and Key Laboratory of Physics and Chemistry of Function Materials, Inner Mongolia, 81 Zhaowudalu, Huhhot 010022, China

ARTICLE INFO

Article history:
Received 29 July 2010
Received in revised form
21 November 2010
Accepted 22 November 2010
Available online 30 November 2010

Keywords:
Magnetite
Magnetic materials
Magnetic measurements
Thermal decomposition

ABSTRACT

An easy synthesis route of magnetite (Fe_3O_4) nanopowder is developed by using thermal decomposition of Fe–urea complex ($[Fe(CON_2H_4)_6](NO_3)_3$). The formation of Fe_3O_4 is confirmed from X-ray powder diffraction (XRD) and X-ray photoelectron spectroscopy (XPS) measurements. The morphological properties and magnetic properties of the Fe_3O_4 are characterized by transmission electron microscopy (TEM) and magnetic measurements, respectively. By an increase in reaction temperature from 200 to 300 °C, the average crystallite size of the Fe_3O_4 nanopowder increases from 37 to 50 nm. Room temperature magnetization hysteresis curves show that the Fe_3O_4 nanopowder possesses ferrimagnetic characteristics. The saturation magnetization of the Fe_3O_4 nanopowder increases from 70.7 to 89.1 emu/g when the reaction temperature increases from 200 to 300 °C.

1. Introduction

Among several iron oxides, magnetite (Fe_3O_4) is a ferrimagnetic material with the highest saturation magnetization (Ms) of 92.0 emu/g. It is readily available and relatively stable under ambient conditions. Owing to these excellent properties, the Fe_3O_4 has been widely used in many applications such as magnetic recording, ferro-fluids, magnetic separation, magnetic resonance imaging, and catalysis for a long time [1–6]. When the particle size of Fe_3O_4 is decreased to nanoscales, it exhibits superparamagnetic behavior [7,8]. This nanosize effect together with biocompatible properties of the material are considered of great potential for applications in biotechnology and biomedicine including bio-assays, magnetic resonance imaging (MRI), magnetically guided drug delivery, and hyperthermia [9–11]. In recent years, the Fe_3O_4 attracts much attention from environmental applications in which it is used as an adsorbent, due to its high adsorption capacity for heavy metals and organic pollutants [12]. Iram et al. reported that Fe_3O_4 hollow nanospheres showed enhanced removal abilities for neutral red dye in wastewater [13]. Mahdavian et al. prepared polymeric-modified Fe_3O_4 nanopowder, and found that this nanopowder possessed large adsorption capacities for heavy metal cations, Cu^{2+}, Pb^{2+}, Ni^{2+}, and Cd^{2+} [14]. Due to its excellent magnetic properties, the Fe_3O_4 is also widely used as a magnetic support of catalysts. For example, it has been demonstrated that Ag/Fe_3O_4 nanocomposite has high catalytic activities for degradation of rhodamine B and epoxidation of styrene [15,16]. The most important advantage of using Fe_3O_4 as adsorbents or magnetic support of catalysts is that it can be easily separated from reaction system with an external magnetic field. For many applications, high quality Fe_3O_4 nanopowder with different properties is required to satisfy individual demand. For example, for biomedical applications, the Fe_3O_4 nanopowder is required to be biocompatible and should possess superparamagnetic characteristics to prevent agglomeration of the particles. For applications in water treatment, however, it is desirable that Fe_3O_4 nanopowder has ferrimagnetic characteristics with a high Ms and high specific surface area.

In response to the many potential applications for Fe_3O_4 nanopowder, various preparation methods have been developed, such as co-precipitation, microemulsion, hydrothermal method, sonochemical approach, mechanochemical approach, and non-aqueous synthetic method, etc. [17–22]. Most of the previously developed methods involve multiple steps and use multi-reagents, which will lead to the large wastage of energy and material. Among these methods, the nonaqueous synthetic method attracts much attention; and, it has been extensively demonstrated that Fe_3O_4 nanopowder with rather narrow size distribution can be obtained by using this technique [23–25]. However, the use of multi-reagents including organometallic compound of iron, organic solvents and some stabilizers are still required in this method. In addition, in most case, iron pentacarbonyl ($Fe(CO)_5$), an extremely toxic and unstable chemical, is commonly used as a precursor, which may

* Corresponding author. Tel.: +86 471 43921214; fax: +86 471 4392124.
E-mail address: asuha42@yahoo.com.cn (S. Asuha).

0925-8388/$ – see front matter © 2010 Elsevier B.V. All rights reserved.
doi:10.1016/j.jallcom.2010.11.145

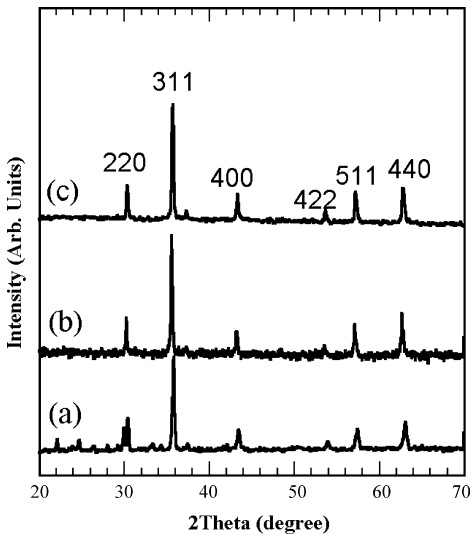

Fig. 1. XRD patterns of the samples prepared by the direct thermal decomposition of $[Fe(CON_2H_4)_6](NO_3)_3$ in a closed container at (a) 200 °C, (b) 250 °C, and (c) 300 °C.

limit the usage of this method for the mass production of Fe_3O_4 nanopowder.

In our previous studies, we found that the direct thermal decomposition of $[Fe(CON_2H_4)_6](NO_3)_3$ in an open container can produce maghemite (γ-Fe_2O_3) nanopowder [26,27]. We also found that Fe_3O_4 nanopowder with superparamagnetic properties can be prepared by a solvothermal method using the iron urea complex as a precursor [28]. In comparison with organic iron complexes (e.g., $Fe(CO)_5$, iron acetylacetonate, iron cupferronates) that are currently used as precursors in thermal decomposition process, the $[Fe(CON_2H_4)_6](NO_3)_3$ is a nontoxic, stable inorganic complex, as has been evidenced from its application in agriculture where it is used as a fertilizer [29]; hence, it can safely be used as a iron oxide precursor. In the present work, we show that Fe_3O_4 nanopowder with ferrimagnetic characteristics can be prepared via the direct thermal decomposition of $[Fe(CON_2H_4)_6](NO_3)_3$ in a closed container. The main advantages of this method are: (i) the preparation procedure involves only one-step, (ii) only one reagent (i.e., $[Fe(CON_2H_4)_6](NO_3)_3$) is used. Accordingly, these advantages are very promising for the large scale production of Fe_3O_4 nanopowder when taking the production cost and the influence of production on environment into consideration.

2. Experimental

2.1. Synthesis

2.0 g of the $[Fe(CON_2H_4)_6](NO_3)_3$, which was synthesized using previously reported method [26], was added to a 45-mL stainless autoclave with a Teflon liner. Then the autoclave was heated in an oven at a predetermined temperature for 2 h, resulting in the formation of a black fine powder.

2.2. Characterization

X-ray diffraction patterns (XRD) were recorded on a Philips PW 1830 diffractometer using CuKα radiation. X-ray photoelectron spectroscopy (XPS) spectra were measured using an AXIS-Ultra instrument from Kratos Analytical with a monochromatic Al Kα radiation source; in this case, peak positions were calibrated using the C 1s peak position. TEM measurements were carried out using a JEOL JEM-2200FS transmission electron microscope. Magnetic measurements were performed using a Lake Shore 7407 vibrating-sample magnetometer (VSM) at room temperature.

3. Results and discussion

Fig. 1 shows the XRD patterns of the samples prepared by the direct thermal decomposition of $[Fe(CON_2H_4)_6](NO_3)_3$ at different temperatures for 2 h. The diffraction patterns match well with the Joint Committee on Powder Diffraction Standards (JCPDS) file of Fe_3O_4. In iron oxides, both Fe_3O_4 and γ-Fe_2O_3 have a same cubic spinel crystalline structure, and it is very difficult to differentiate them with XRD patterns. But they can be distinguished using *d*-spacing values. The *d*-spacing values of the sample which was obtained at 250 °C together with the JCPDS files of Fe_3O_4 and γ-Fe_2O_3 are listed in Table 1. It can be seen that experimental data match with the *d*-spacing values of Fe_3O_4 better, indicating the formation of Fe_3O_4. For the samples prepared at 200, 250 and 300 °C, the average crystallite sizes of Fe_3O_4, which were calculated from the half-width of diffraction lines by using Scherrer's equation, were estimated to be 37, 42 and 50 nm, respectively, indicating that Fe_3O_4 crystallite size increased with the increase of reaction temperature. Although the crystallite size could be controlled by varying reaction temperature, the controllable range was relatively narrow. One advantage of this method is that the Fe_3O_4 nanopowder with a relatively large particle size can be prepared in a short time as compared with our previously reported method [28].

Table 1
d-Spacings of the sample prepared by the direct thermal decomposition of $[Fe(CON_2H_4)_6](NO_3)_3$ in a closed container at 250 °C and those of Fe_3O_4 and γ-Fe_2O_3 from JCPDS files.

d (Å)	Fe_3O_4 (Å)[a]	γ-Fe_2O_3 (Å)[b]	*hkl*
2.9541	2.9670	2.9530	220
2.5226	2.5320	2.5177	311
2.0923	2.0993	2.0866	400
1.7102	1.7146	1.7045	422
1.6121	1.6158	1.6073	511
1.4812	1.4845	1.4458	440

[a] JCPDS file No. 19-629.
[b] JCPDS file No. 39-1346.

As reported in literatures [30], XPS has also been proven to be a powerful tool for the discrimination of Fe_3O_4 and γ-Fe_2O_3. Therefore, the XPS spectra of the sample have been measured in order to further confirm the formation of Fe_3O_4. Fig. 2 shows XPS spectrum in the Fe 2p region for the sample prepared by the direct thermal decomposition of $[Fe(CON_2H_4)_6](NO_3)_3$ at 250 °C for 2 h (spectrum a). For comparison, the spectrum for γ-Fe_2O_3, which is prepared by previously reported method [26], is also shown in the figure (spectrum b). For present sample, the peak positions of Fe $2p_{3/2}$ and Fe $2p_{1/2}$ were observed at 710.7 and 724.2 eV, respectively, which agree well with those for the Fe_3O_4 reported in literature [31]. On the other hand, the peak positions of Fe $2p_{3/2}$ and Fe $2p_{1/2}$ for γ-

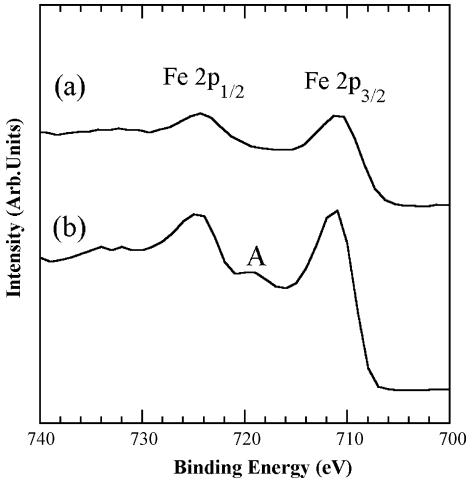

Fig. 2. XPS spectra: (a) for the sample prepared by the direct thermal decomposition of $[Fe(CON_2H_4)_6](NO_3)_3$ in a closed container at 250 °C for 2 h, and (b) for γ-Fe_2O_3.

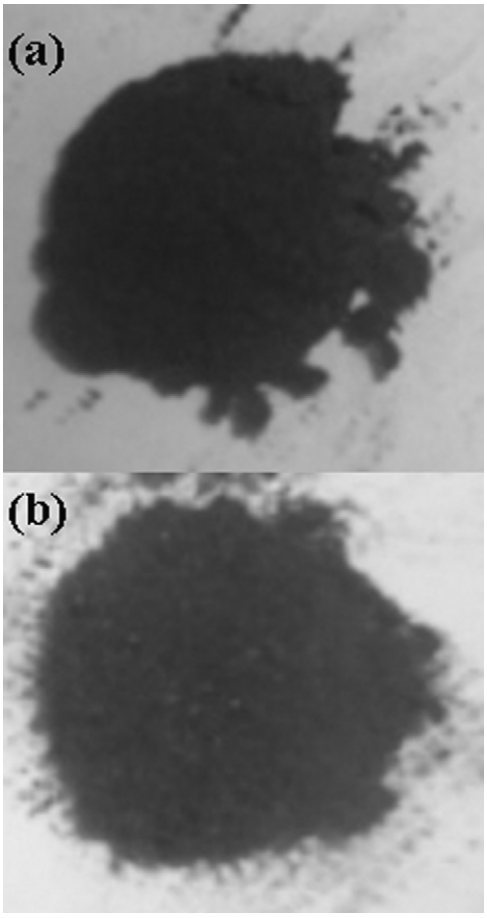

Fig. 3. Photographs: (a) for the sample prepared by the direct thermal decomposition of $[Fe(CON_2H_4)_6](NO_3)_3$ in a closed container at 250 °C for 2 h, and (b) for γ-Fe_2O_3.

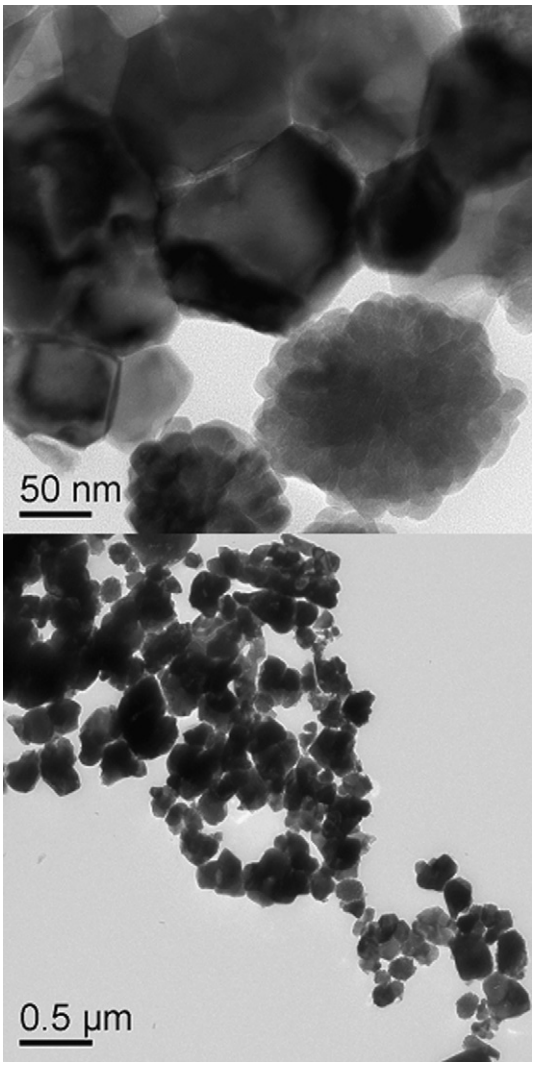

Fig. 4. TEM micrographs of Fe_3O_4 nanopowder prepared by the direct thermal decomposition of $[Fe(CON_2H_4)_6](NO_3)_3$ at 250 °C for 2 h.

Fe_2O_3 were 711.3 and 724.6 eV, respectively. Beside peak position, the appearance of satellite peak of Fe $2p_{3/2}$ is also one important feature that could be used for the discrimination of Fe_3O_4 and γ-Fe_2O_3. According to previous studies, the Fe $2p_{3/2}$ for Fe_3O_4 does not have any satellite peaks, while that for γ-Fe_2O_3 has a satellite peak at ~719 eV [30,31]. As seen in Fig. 2, a satellite peak was present in the spectrum (b) (denoted by A in the figure), while the satellite peak was absent in the spectrum (a), indicating the formation of Fe_3O_4 in the present sample. Another distinguishable feature of these oxides is that they have quite different colors. Fig. 3 shows the photograph of the Fe_3O_4 nanopowder. For comparison, the photograph of γ-Fe_2O_3 nanopowder is also shown in the figure. Fe_3O_4 was black, while γ-Fe_2O_3 was red-brown, which further confirms the formation of Fe_3O_4 in the present sample. The TEM micrographs of Fe_3O_4 nanopowder prepared by the direct thermal decomposition of $[Fe(CON_2H_4)_6](NO_3)_3$ at 250 °C for 2 h are shown in Fig. 4. It is clearly seen that the Fe_3O_4 particles do not have a defined shape (cf. high-magnification image). In addition, the sizes of individual particles were considerably larger than the average crystallite size estimated from XRD data, probably due to the agglomeration of primary particles. As seen in the low-magnification image, these individual particles were further agglomerated into larger aggregates in different sizes.

The formation mechanism of Fe_3O_4 can be understood from the thermal decomposition reaction of $[Fe(CON_2H_4)_6](NO_3)_3$. According to our previous study, the thermal decomposition of $[Fe(CON_2H_4)_6](NO_3)_3$ involves a two-stage decomposition process; and, $Fe(NO_3)_3$ and CON_2H_4 are the main products in the first step [27]. The products of the second stage are likely to depend on heat treatment atmosphere. In the present case where the thermal decomposition of $[Fe(CON_2H_4)_6](NO_3)_3$ proceeds in a closed container, the released CON_2H_4 in the first stage could not escape from the reactor by evaporation; hence, it can partially reduce Fe^{3+} to Fe^{2+}, leading to the formation of Fe_3O_4:

$$3Fe(NO_3)_3 + CON_2H_4 \rightarrow Fe_3O_4 + CO_2 + 4NO + 7NO_2 + O_2 + 2H_2O \quad (1)$$

When $[Fe(CON_2H_4)_6](NO_3)_3$ is heated in an open container (i.e., in air), however, the released CON_2H_4 in the first stage will be separated from $Fe(NO_3)_3$ by evaporation; hence, the reduction of Fe^{3+} does not occur, which results in the formation of γ-Fe_2O_3. In this case, even if the Fe_3O_4 formed in the second step, it will be quickly oxidized by air into γ-Fe_2O_3. Consequently, the thermal decomposition of $[Fe(CON_2H_4)_6](NO_3)_3$ in an open container will yield γ-Fe_2O_3, as evidenced from our previous studies [26]. Lupin et al. also studied the thermal decomposition of $[Fe(CON_2H_4)_6](NO_3)_3$ in different atmospheres, and reported that the thermal decomposition of $[Fe(CON_2H_4)_6](NO_3)_3$ in argon could produce Fe_3O_4 [29]. But in that case, the formation mechanism of Fe_3O_4 is quite different from that proposed in the present work.

It is clear from above discussions that the formation conditions of Fe_3O_4 and γ-Fe_2O_3 nanopowder are quite different. The formation of pure Fe_3O_4 or γ-Fe_2O_3 nanopowder depends on atmosphere

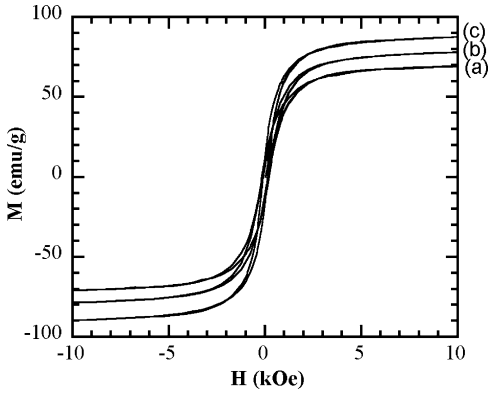

Fig. 5. Magnetization curves of the samples prepared by the direct thermal decomposition of $[Fe(CON_2H_4)_6](NO_3)_3$ in a closed container at (a) 200 °C, (b) 250 °C, and (c) 300 °C.

in which the thermal decomposition of $[Fe(CON_2H_4)_6](NO_3)_3$ is carried out. On the other hand, it is probable that both Fe_3O_4 and γ-Fe_2O_3 nanopowder can be formed simultaneously by using this method. In this case, a separation process is needed to obtain pure oxide, which is still a challenging research subject. Besides Fe_3O_4, as shown in the reaction formula (1), toxic NO and NO_2 are also formed as by-products in the thermal decomposition process of $[Fe(CON_2H_4)_6](NO_3)_3$. This environmental problem should be taken into account when the method is employed to the mass production of Fe_3O_4.

Fig. 5 shows the room temperature magnetization hysteresis curves of the samples prepared by the direct thermal decomposition of $[Fe(CON_2H_4)_6](NO_3)_3$ at different temperatures for 2 h. Each hysteresis curve had a certain value of coercivity and remanent magnetization (e.g., 138 Oe and 7.5 emu/g for the sample prepared at 250 °C), indicating that the Fe_3O_4 nanopowder have ferrimagnetic characteristics. The saturation magnetization (Ms) were 70.7, 79.4 and 89.1 emu/g for the samples prepared at 200, 250 and 300 °C, respectively, showing that the Ms increased with the increase in reaction temperature or Fe_3O_4 crystallite size. The maximum Ms was considerably larger than that of bulk γ-Fe_2O_3 crystallite (i.e., 73.5 emu/g) and slightly smaller than that of bulk Fe_3O_4 crystallite (i.e., 92.0 emu/g). The magnetic properties of the Fe_3O_4 nanopowder were quite different from those of Fe_3O_4 nanopowder obtained in our previous study [28]. The difference in the magnetic properties of the Fe_3O_4 nanopowder produced by the two methods mainly results from the difference in Fe_3O_4 particle size. Due to relatively large particle size, the Fe_3O_4 nanopowder obtained in the present work showed ferrimagnetic characteristics; while that obtained in the previous work exhibited superparamagnetic properties because of small particle size. Fe_3O_4 is a ferrimagnetic material; but, when its particle size is decreased to a small value, it will become superparamagnetic. It is reported that the critical particle size at which the Fe_3O_4 becomes superparamagnetic is around 29 nm [8]; therefore, the results obtained in our present and previous studies are in good agreement with the result.

For applications in biotechnology and biomedicine, Fe_3O_4 powder is required to be dispersive in a medium. We have investigated the dispersibility of the present Fe_3O_4 in some solvents (e.g., H_2O, C_2H_5OH); however, it does not have a good dispersibility in these media, probably due to the large particle size and the low concentration of surface exchange sites on the Fe_3O_4. Therefore, both lowering particle size and surface modification processes will be required to improve the dispersibility of the Fe_3O_4.

4. Conclusions

In conclusion, this work demonstrates that the Fe_3O_4 nanopowder with ferrimagnetic property can be prepared by the direct thermal decomposition of $[Fe(CON_2H_4)_6](NO_3)_3$ in a closed container. As a reducing agent, the CON_2H_4, which is one of the products of thermal decomposition of $[Fe(CON_2H_4)_6](NO_3)_3$, play an important role in the Fe_3O_4 formation process; it cause the partial reduction of Fe^{3+} to Fe^{2+}, leading to the formation of Fe_3O_4. The present method can produce Fe_3O_4 nanopowder with a relatively large saturation magnetization, and the Fe_3O_4 particle size can be controlled by varying reaction temperature. The saturation magnetization of the Fe_3O_4 nanopowder strongly depends on the Fe_3O_4 crystallite size. The proposed method is easy and reproducible. Owing to these advantages, this method is quite promising for the mass production of Fe_3O_4 nanopowder.

Acknowledgments

This work was financially supported by National Natural Science Foundation of China (Grant No. 20861006) and Natural Science Foundation of Inner Mongolia (Grant No. MS0806).

References

[1] K. Yamaguchi, K. Matsumoto, T. Fujii, J. Appl. Phys. 67 (1990) 4493–4495.
[2] R. Kaiser, G. Miskolcze, J. Appl. Phys. 41 (1970) 1064–1072.
[3] Z.M. Saiyed, M. Parasramka, S.D. Telang, C.N. Ramchand, Anal. Biochem. 363 (2007) 288–290.
[4] A.K. Guptaa, M. Gupta, Biomaterials 26 (2005) 3995–4021.
[5] S. Guo, D. Li, L. Zhang, J. Li, E. Wang, Biomaterials 30 (2009) 1881–1889.
[6] D.H. Zhang, G.D. Li, J.X. Li, J.S. Chen, Chem. Commun. (2008) 3414–3416.
[7] G.F. Goya, T.S. Berquo, F.C. Fonseca, J. Appl. Phys. 94 (2003) 3520–3527.
[8] A. Angermann, J. Töpfer, J. Mater. Sci. 43 (2008) 5123–5130.
[9] P. Majewski, B. Thierry, Crit. Rev. Solid State Mater. Sci. 32 (2007) 203–215.
[10] Y. Lin, C. Haynes, Chem. Mater. 21 (2009) 3979–3986.
[11] R. Hao, R. Xing, Z. Xu, Y. Hou, S. Gao, S. Sun, Adv. Mater. 22 (2010) 2729–2742.
[12] J.T. Mayo, C. Yavuz, S. Yean, L. Cong, H. Shipley, W. Yu, J. Falkner, A. Kan, M. Tomson, V.L. Colvin, Sci. Technol. Adv. Mater. 8 (2007) 71–75.
[13] M. Iram, C. Guo, Y. Guan, A. Ishfaq, H. Liu, J. Hazard. Mater. 181 (2010) 1039–1050.
[14] A.R. Mahdavian, M.A.-S. Mirrahimi, Chem. Eng. J. 159 (2010) 264–271.
[15] X. Zhang, W. Jiang, X. Gong, Z. Zhang, J. Alloys Compd. 508 (2010) 400–405.
[16] D. Zhang, G. Li, J. Lia, J. Chen, Chem. Commun. (2008) 3414–3416.
[17] R.A. Frimpong, J. Dou, M. Pechan, J.Z. Hilt, J. Magn. Magn. Mater. 322 (2010) 326–331.
[18] Z.H. Zhou, J. Wang, X. Liu, H.S.O. Chan, J. Mater. Chem. 11 (2001) 1704–1709.
[19] S. Ni, X. Wang, G. Zhou, F. Yang, J. Wang, Q. Wang, D. He, J. Alloys Compd. 505 (2010) 727–732.
[20] R. Vijayakumar, Y. Koltypin, I. Felner, A. Gedanken, Mater. Sci. Eng. A 286 (2000) 101–105.
[21] C.R. Lin, Y.M. Chu, S.C. Wang, Mater. Lett. 60 (2006) 447–450.
[22] S. Sun, H. Zeng, J. Am. Chem. Soc. 124 (2002) 8204–8205.
[23] R. Shi, X. Liu, G. Gao, R. Yi, G. Qiu, J. Alloys Compd. 485 (2009) 548–553.
[24] D. Li, D. Jiang, M. Chen, J. Xie, Y. Wu, S. Dang, J. Zhang, Mater. Lett. 64 (2010) 2462–2464.
[25] D. Maity, S.N. Kale, R. Kaul-Ghanekar, J.M. Xue, J. Ding, J. Magn. Magn. Mater. 321 (2009) 3093–3098.
[26] S. Asuha, S. Zhao, H.Y. Wu, L. Song, O. Tegus, J. Alloys Compd. 472 (2009) L23–L24.
[27] S. Zhao, H.Y. Wu, L. Song, O. Tegus, S. Asuha, J. Mater. Sci. 44 (2009) 926–930.
[28] S. Zhao, S. Asuha, Powder Technol. 197 (2010) 295–297.
[29] M.S. Lupin, G.E. Peters, Thermochim. Acta 73 (1984) 79–87.
[30] C. Ruby, B. Humbert, J. Fusy, Surf. Interface Anal. 29 (2000) 377–380.
[31] T. Yamashita, P. Hayes, Appl. Surf. Sci. 254 (2008) 2441–2449.